Influence of *3d*-*4f* interactions in the magnetic phases of $R\mathrm{Fe}_x\mathrm{Mn}_{12-x}$ ($R=$ Gd, Tb, and Dy) compounds: Coexistence of ferromagnetism and antiferromagnetism at different crystallographic sites

C. Piqué,[1,*] J. A. Blanco,[1] R. Burriel,[2] E. Abad,[1] M. Artigas,[2] and M. T. Fernández-Díaz[3]

[1]*Departamento de Física, Universidad de Oviedo, 33007 Oviedo, Spain*
[2]*Instituto de Ciencia de Materiales de Aragón, CSIC, Universidad de Zaragoza, 50009 Zaragoza, Spain*
[3]*Institut Laue-Langevin, 38042 Grenoble, France*

The structural and magnetic properties of tetragonal $R\mathrm{Fe}_x\mathrm{Mn}_{12-x}$ ($R=$ Gd, Tb, Dy) compounds have been extensively studied by means of dc and ac susceptibilities, x-ray absorption spectroscopy at Gd-L_{III} edge, and neutron-powder-diffraction experiments. The substitution of Fe for Mn in $R\mathrm{Fe}_x\mathrm{Mn}_{12-x}$ not only influences the magnetic interactions on the *3d* sublattice (the Néel temperature doubles, going from $x=0$ to $x=6$, and the compounds become ferromagnetic for $x=8$ with Curie temperatures of around 300 K), but also has a major effect on the magnetism of R. While in pure $R\mathrm{Mn}_{12}$ the ordering temperatures of R, through R-R interactions, are close to liquid-helium temperatures, the substitution of Mn by Fe leads to the appearance of spin-glass-like behavior as well as to magnetic polarization effects between the *3d* and *4f* sublattices, together with the disappearance of the cooperative ordering of the R sublattice. This polarization is able to induce *4f* magnetic moments below 150 K. In addition, the *3d* magnetic interactions are modified by the presence of magnetic R ions in the system: both ferromagnetic and antiferromagnetic orderings are observed simultaneously over different crystallographic sites. A general analysis of the available experimental data allows us to establish the magnetic phase diagram of $R\mathrm{Fe}_x\mathrm{Mn}_{12-x}$.

I. INTRODUCTION

Rare-earth intermetallic compounds are of almost unlimited richness for the study of *3d* and *4f* magnetism and the interplay between them. At the same time, their potential applications explain the considerable attention paid to these materials. In $R\mathrm{Mn}_{12}$ (R is a rare earth) compounds, the Mn ions are coupled antiferromagnetically showing Néel temperatures of around 100 K. The magnetic-moment arrangement is such that it cancels the effects of eventual R-Mn exchange interactions on the rare-earth site. The magnetic R ions order at low temperatures (below 5 K) only through R-R exchange interactions, leading to two distinct ordering temperatures in the compounds, which is not usual for materials of this type.[1,2] In most of the studied intermetallic alloys, the *3d* subsystem produces a strong exchange field acting on the rare earth and all the magnetic sublattices order at the same time. However, other systems presenting small values of the *3d*-*4f* exchange interaction show two transition temperatures, like $R\mathrm{Fe}_4\mathrm{Al}_8$,[3] with the same ThMn_{12}-type structure. In these systems, Fe orders at 100–200 K in a modulated antiferromagnetic structure that produces a very small molecular field on the rare earth. R becomes slightly polarized (shown by x-ray resonant magnetic scattering).[4] In the range 10–35 K, the R magnetic ordering takes place, but it does not originate from R-R interactions, which are weak in this series.

Fe dilution in $R\mathrm{Mn}_{12}$ compounds at low ratios can lead to a system with conveniently small *3d*-*4f* exchange interaction to study the competition with *4f*-*4f* interactions and magnetocrystalline anisotropy. We started our research work with a nonmagnetic ion as Y.[5] However, in the present paper, carried out in connection with a heat-capacity study,[6] we have extended the study to Gd, Tb, and Dy. The $L=0$ character of the $4f^7$ shell of Gd provides only a minor influence to the crystalline electric fields (CEFs). Hence, the magnetic properties are determined essentially by exchange interactions. In the compounds with Tb and Dy, crystalline-electric-field effects will be investigated.

Other studies in the series $R\mathrm{Fe}_x\mathrm{Mn}_{12-x}$ with $R=$ Ho,[7–9] Er, and Nd (Refs. 8, 10, and 11) have proposed the existence of several magnetic phenomena: ordering of the *3d* ferromagnetic (F) or antiferromagnetic (AF) sublattice, depending on composition, change from F to (AF+F) ordering at low temperatures, or ordering of the R sublattice. Besides, intermediate compositions show the disappearance of the long-range ordering on the R sublattice and of some magnetic components on different *3d* sites, indicating spin-glass behavior.

To ascertain experimentally how the long-range order develops in $R\mathrm{Fe}_x\mathrm{Mn}_{12-x}$, we undertook a general analysis using dc and ac susceptibilities, heat capacity,[6] x-ray-absorption spectroscopy at the Gd-L_{III} edge, and neutron-powder-diffraction experiments.

II. EXPERIMENT DETAILS

Polycrystalline samples of composition $R\mathrm{Fe}_x\mathrm{Mn}_{12-x}$ [$R=$ Gd ($x=2$, 4, and 6), Tb ($x=0$, 2, 4, 6, and 8), Dy ($x=0$, 2, 4, 6, and 8)] were prepared by induction melting of the constituent elements using an excess of Mn due to the high Mn vapor pressure. These samples were annealed at 1000 °C for 5 days in argon atmosphere. They were subsequently checked for phase purity by x-ray powder diffraction on a high-resolution SEIFERT-XRD-3000 diffractometer at the University of Oviedo. In the TbMn_{12} sample, β-Mn (12%)

TABLE I. Refined structural parameters for $R\mathrm{Fe}_x\mathrm{Mn}_{12-x}$ at room temperature from neutron-diffraction experiments for $R=$Tb, Dy, and from x-ray diffraction for $R=$Gd. Refined Fe composition, x_{ref}; distribution of the Fe content on the three transition-metal sites $8i$, $8j$, and $8f$; fractional position coordinates; lattice parameters a and c; nearest-neighbor (nn) distances between the rare-earth site, $2a$, and the three sites $8i$, $8j$ and $8f$; and reliability factor, R_B^N.

		%Fe			Coordinates		Lattice parameters		nn distance (Å)			R_B^N
	x_{ref}	$8i$	$8j$	$8f$	$x(8i)$	$x(8j)$	a (Å)	c (Å)	$2a$-$8i$	$2a$-$8j$	$2a$-$8f$	(%)
$\mathrm{GdFe_2Mn_{10}}$					0.364(1)	0.276(1)	8.612(2)	4.782(2)	3.11	3.06	3.27	10.4
$\mathrm{GdFe_4Mn_8}$					0.364(1)	0.282(3)	8.583(2)	4.781(2)	3.12	3.05	3.26	13.2
$\mathrm{GdFe_6Mn_6}$					0.364(1)	0.279(1)	8.556(2)	4.780(2)	3.08	3.05	3.23	10.0
$\mathrm{TbMn_{12}}$					0.360(1)	0.271(1)	8.551(4)	4.730(3)	3.09	3.04	3.25	12.8
$\mathrm{TbFe_2Mn_{10}}$	2.0(1)	2.0(4)	14.4(4)	32.8(4)	0.358(1)	0.279(2)	8.548(1)	4.751(1)	3.06	3.04	3.25	4.5
$\mathrm{TbFe_4Mn_8}$	4.1(1)	9.2(3)	35.9(2)	58.5(3)	0.364(1)	0.271(3)	8.536(1)	4.759(1)	3.11	3.08	3.24	6.3
$\mathrm{TbFe_6Mn_6}$	6.0(1)	17.0(6)	57.3(6)	76.7(6)	0.358(2)	0.277(1)	8.508(1)	4.758(1)	3.05	3.04	3.23	4.7
$\mathrm{TbFe_8Mn_4}$	8.2(1)	39.2(4)	76.8(8)	88.4(8)	0.367(4)	0.280(1)	8.460(1)	4.754(1)	3.10	3.02	3.22	4.7
$\mathrm{DyFe_2Mn_{10}}$	2.8(1)	10.0(8)	20.0(4)	38.0(8)	0.362(3)	0.269(9)	8.525(4)	4.745(3)	3.13	3.10	3.24	12.4
$\mathrm{DyFe_4Mn_8}$	4.3(1)	11.2(4)	37.2(4)	60.0(8)	0.365(3)	0.287(5)	8.509(1)	4.748(1)	3.15	3.02	3.23	6.4
$\mathrm{DyFe_6Mn_6}$	6.1(1)	22.8(8)	56.8(8)	73.0(1)	0.380(9)	0.277(2)	8.487(1)	4.750(1)	3.30	3.03	3.23	6.3
$\mathrm{DyFe_8Mn_4}$	8.0(1)	38.0(4)	75.6(8)	85.6(4)	0.352(4)	0.277(1)	8.468(1)	4.751(1)	2.99	3.04	3.22	5.0

and a small amount of $\mathrm{Tb_6Mn_{23}}$ (less than 0.5%) were detected, as occurred in Y and Er compounds.[5,8] The $R_6\mathrm{(FeMn)_{23}}$ phase was not present in the ternary compounds, while the amount of β-Mn decreased with increasing Fe concentration.

dc and ac susceptibilities were measured in a Quantum Design superconducting quantum interference device magnetometer at the University of Zaragoza and the University of País Vasco.

Neutron-diffraction spectra were collected at the ILL (Grenoble, France) using the D1B diffractometer with a neutron wavelength $\lambda=2.52$ Å (for Tb and Dy compounds) and the D4 diffractometer with $\lambda=0.50$ Å (for Gd compounds, because of the high absorption of Gd for the D1B wavelength). We used a double walled vanadium cylinder sample holder (5 cm height, 5 cm outer diameter, and 1 mm annular thickness) for the Dy samples to reduce neutron absorption. For these samples, the neutron-powder-diffraction patterns were refined allowing the Dy occupation number to be variable in order to describe the experimental spectra in the paramagnetic phase. This Dy occupation number was then fixed for the refinements of the magnetic phase at 1.5 K. Rietveld refinements were carried out using the FULLPROF program.[12] Finally, x-ray-absorption spectra (XAS) were recorded at beamline 7.1 at SRS (Daresbury). The storage ring was operated at 2 GeV with an average current of 150 mA. XAS experiments were collected working within the usual transmission geometry with homogeneous thin layers of the powdered samples at the Gd-L_{III} edge. We used a double-crystal Si (111) monochromator in order to obtain a harmonic rejection of about 50% by slightly detuning the second crystal from the collinear alignment. XAS were analyzed according to standard procedures and normalized to the absorption coefficient at around 100 eV above the edge to eliminate thickness dependence.

III. RESULTS AND DISCUSSION

A. Structural properties

All the $R\mathrm{Fe}_x\mathrm{Mn}_{12-x}$ samples were found to crystallize in a body-centered-tetragonal structure ($\mathrm{ThMn_{12}}$-type) possessing a $I4/mmm$ space group, with the rare earth occupying the $2a$ Wyckoff position and the transition metals lying at the $8i$, $8j$, and $8f$ positions. The main crystallographic data of the investigated compounds at room temperature were refined from the neutron-diffraction patterns (except for Gd compounds, for which x-ray diffraction was used) and are shown in Table I. The site occupancies show that Fe prefers to occupy the $8f$ site, whereas Mn is found preferentially at the $8i$ sites, irrespective of the rare earth, as previously found for the Er,[8] Ho,[9] and Y (Refs. 5 and 9) series. The cell parameters a and c show the same behavior as in the Y series with Fe concentration and with temperature.[5] In the case of $\mathrm{DyFe_8Mn_4}$, the a cell parameter decreases up to 50 K and then increases, the compound undergoing a spin reorientation phase transition around this temperature (see below).

B. Magnetic properties

The temperature dependences of the dc susceptibility M/H of $\mathrm{TbFe}_x\mathrm{Mn}_{12-x}$, $\mathrm{DyFe}_x\mathrm{Mn}_{12-x}$, and $\mathrm{GdFe}_x\mathrm{Mn}_{12-x}$ are shown in Figs. 1, 2, and 3, respectively, for x between 0 and 6, while Figs. 4 and 5 present the dc and ac susceptibilities for $\mathrm{TbFe_8Mn_4}$ and $\mathrm{DyFe_8Mn_4}$.

In the case of the binary compound $\mathrm{TbMn_{12}}$, we observe a rapid increase in M/H at low temperatures, saturating at $T_R=4.5$ K (see Fig. 1). This indicates the cooperative ferromagnetic ordering of the Tb sublattice due to Tb-Tb exchange interaction, in agreement with previous results found by others authors[1,2] and the heat-capacity study.[6] This heat-capacity study also gives 120 K as the Néel temperature,
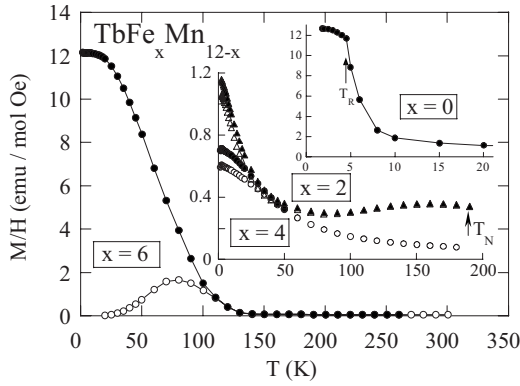
FIG. 1. Temperature dependence of the dc susceptibility M/H for TbFe$_x$Mn$_{12-x}$ [x=0, 2 (triangles), 4, and 6] in ZFC (open markers) and FC (solid markers) conditions, under an applied field of 0.5 kOe. T_R is the ordering temperature of the rare-earth sublattice and T_N the Néel temperature. The lines are guides for the eye.

where the Mn atoms order antiferromagnetically. In the case of DyMn$_{12}$, we also observe a rapid increase in M/H at low temperatures, though without reaching a saturation value down to the lowest temperature measured, 1.8 K.

With a small amount of Fe in the sample (x=2 and 4), Tb and Dy ions do not order (see Fig. 1 for Tb and Fig. 2 for Dy), the value of the M/H ratio being similar to that found for the corresponding AF Y compound.[5] The AF ordering of the 3*d* sublattice takes place at T_N (the Néel temperatures in TbFe$_x$Mn$_{12-x}$ are 193 and 232 K for the concentrations x=2 and 4, respectively, these values being taken from the heat-capacity study).[6] In addition, we observe small differences between the zero-field-cooled (ZFC) and field-cooled (FC) magnetization curves (see Fig. 1 and inset on Fig. 2 for DyFe$_4$Mn$_8$ below 4 K). In Fig. 6, the temperature dependence of the ac susceptibility for DyFe$_4$Mn$_8$ shows a peak centered around 4 K for ν=10 Hz. This peak is shifted to a higher temperature with increasing frequency [see Fig. 6(a)]; moreover, the anomaly is strongly reduced by the application
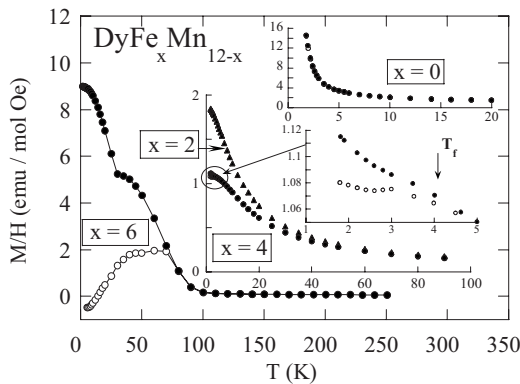
of 10 kOe [see Fig. 6(b)]. These features are characteristic of a spin-glass-like behavior. The spin-freezing temperatures (defined as the cusp in the ac susceptibility) are plotted against $1/\ln(\nu_0/\nu)$ in the inset of Fig. 6(a). From this figure, it can be seen that the slowing down of the dynamics follows a Vogel-Fulcher law. From the fit, T_f is estimated to be around 4 K. This spin-glass behavior is associated with the rare earth due to the low value of the freezing temperature T_f, in contrast with Y compounds where spin-glass behavior has been found in the 3*d* sublattice. The 3*d* spin-glass behavior seems to be related to the differences observed in the ZFC and FC magnetization measurements below 50 K in TbFe$_4$Mn$_8$ and TbFe$_2$Mn$_{10}$ compounds.

However, as can be seen in Fig. 3, in the case of Gd compounds the increase in magnetization is not abrupt for

FIG. 3. Temperature dependence of the dc susceptibility M/H for GdFe$_x$Mn$_{12-x}$ (x=2, 4, and 6) in ZFC and FC conditions, under an applied field of 0.5 kOe. The lines are guides for the eye.

FIG. 2. Temperature dependence of the dc susceptibility M/H for DyFe$_x$Mn$_{12-x}$ [x=0, 2 (triangles), 4, and 6] in ZFC (open markers) and FC (solid markers) conditions, under an applied field of 0.5 kOe. T_f is the spin-freezing temperature. The inset is an amplified view of the low-temperature region for x=4. The lines are guides for the eye.
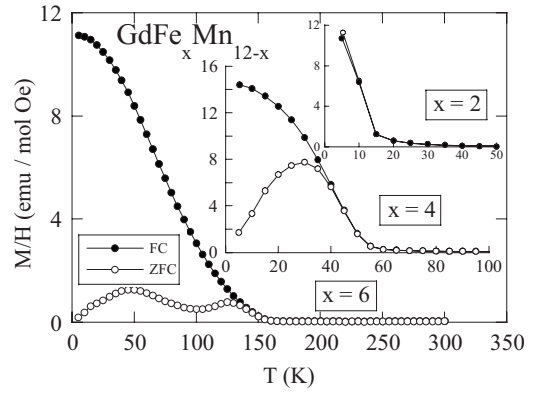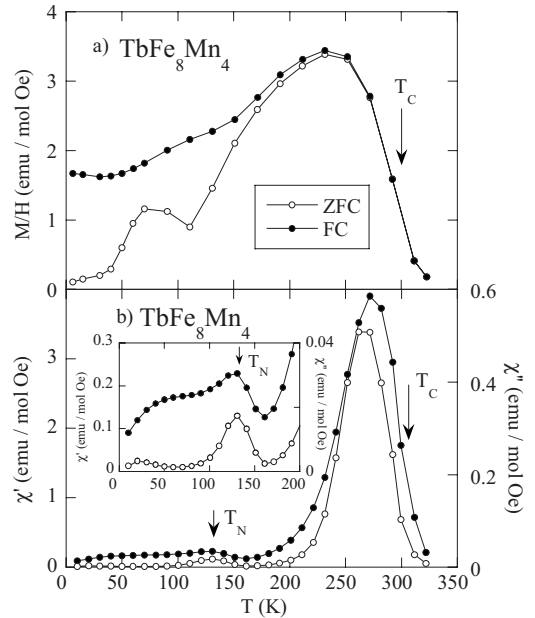

FIG. 4. Temperature dependence (a) of the dc susceptibility for TbFe$_8$Mn$_4$ in ZFC and FC conditions, under an applied field of 1 kOe, and (b) of the real (●) and imaginary (○) parts of the ac magnetic susceptibility. T_C is the Curie temperature and T_N the Néel temperature. The lines are guides for the eye.
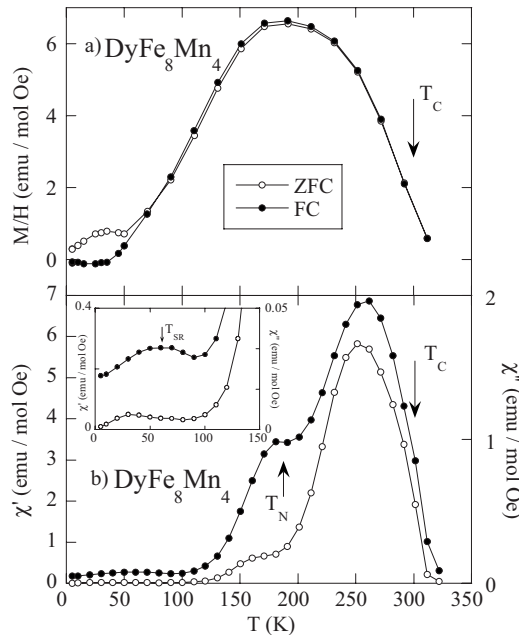
FIG. 5. Temperature dependence (a) of the dc susceptibility for DyFe$_8$Mn$_4$ in ZFC and FC conditions, under an applied field of 1 kOe, and (b) of the real ($\bullet$) and imaginary ($\bigcirc$) parts of the ac magnetic susceptibility. T_C is the Curie temperature, T_N the Néel temperature, and T_{SR} the spin reorientation temperature. The lines are guides for the eye.

$x=4$ and 6 and starts at a temperature that increases with the Fe concentration ($\sim$20, 60, and 150 K for $x=2$, 4, and 6, respectively). This is also the case for TbFe$_6$Mn$_6$ ($\sim$120 K, see Fig. 1) and DyFe$_6$Mn$_6$ ($\sim$100 K, see Fig. 2). This temperature is 1 order of magnitude higher than T_R in the binary

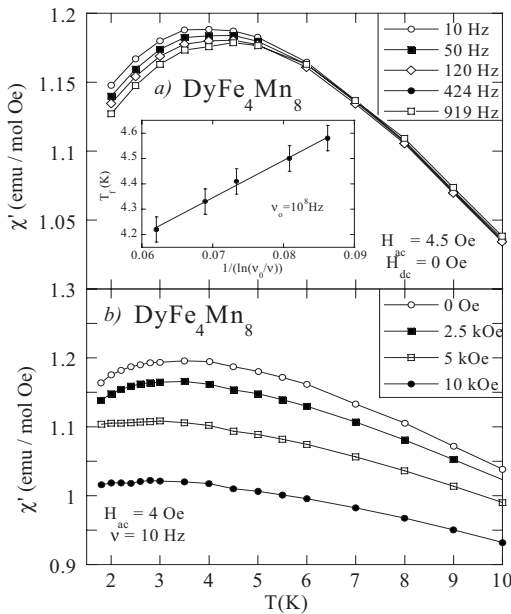

FIG. 6. Temperature dependence of the real part of the ac magnetic susceptibility for DyFe$_4$Mn$_8$ for different (a) frequencies and (b) dc magnetic fields. The lines are guides for the eye.

compounds and its magnitude is directly proportional to the molecular fields acting on the R magnetic moments.[6] The rare earth is polarized by the 3d sublattice, as clearly observed by means of neutron diffraction (see below) and confirmed by the heat-capacity study,[6] where no order-disorder anomaly is observed (we only have a λ anomaly in TbMn$_{12}$), a noncooperative Schottky-type anomaly being found instead. The AF ordering temperature in GdFe$_x$Mn$_{12-x}$ (197, 234, and 223 K for $x=2$, 4, and 6, respectively)[6] is not detected in these magnetic measurements due to the rare-earth paramagnetic contribution. Different values of M/H are found in GdFe$_x$Mn$_{12-x}$ ($x=4$ and 6), TbFe$_6$Mn$_6$ and DyFe$_6$Mn$_6$ for FC and ZFC measurements. This means that the ferrimagnetic order observed in neutron-diffraction measurements (see below) seems to be due to a mutual polarization of the rare earth and the 3d sublattices. In addition, there is a decrease in M/H in the ZFC curves with intermediate maxima. These features can be explained on the basis of ferrimagnetic phenomena, since the magnetization of the different sublattices increases at different rates with decreasing temperature, which leads to the existence of compensation points (see below). In DyFe$_6$Mn$_6$ (see Fig. 2), we observe a negative magnetization below 13 K related to the existence of a compensation point as observed in HoFe$_{7.2}$Mn$_{4.8}$.[7,9] The feature at 30 K in the DyFe$_6$Mn$_6$ FC magnetization curve requires more experimental work in order to ascertain its origin.

The M/H temperature variation for TbFe$_8$Mn$_4$ [Fig. 4(a)] and for DyFe$_8$Mn$_4$ [Fig. 5(a)] also shows the effect of ferrimagnetic behavior below the ordering temperature (T_C=300 K). The anomalies at about 100 K for the Tb compound and at about 50 K in Dy may be explained by the existence of compensation points at these temperatures (from neutron experiments). The ac susceptibility is presented in Fig. 4(b) for TbFe$_8$Mn$_4$ and in Fig. 5(b) for DyFe$_8$Mn$_4$, measured under an ac magnetic field of 4.5 Oe at 10 Hz. The anomaly corresponding to T_C is less extended in temperature than the analogous one in YFe$_8$Mn$_4$, while the anomaly at about 130 K (for Tb) or 180 K (for Dy) is observed in both real and imaginary components of the ac susceptibility, contrary to the case of YFe$_8$Mn$_4$,[5] in which it was only observed in the real part of χ_{ac}. The reason could be the different origin of this anomaly. In the Tb and Dy compounds it corresponds to the AF ordering of the 8i magnetic moment (T_N), as we will show in the neutron-diffraction experiments (see below), while in the Y compound it is associated with the appearance of an AF component in the basal plane in all the 3d sites (8i, 8j, and 8f), due to a continuous reorientation of the magnetic moments from the c axis to the basal plane below 150 K (T_t). In DyFe$_8$Mn$_4$, we also observe a bump at about 60 K that, in view of subsequent neutron-diffraction experiments, we ascribe to a spin reorientation transition.

In order to study all this rich array of phenomena and get a better insight into the aforementioned magnetic behavior in RFe$_x$Mn$_{12-x}$ alloys ($R=$Gd,Tb,Dy), neutron-diffraction experiments were performed to determine the magnetic structure and its evolution with temperature. Typical neutron-diffraction patterns of GdFe$_6$Mn$_6$, TbFe$_4$Mn$_8$, and DyFe$_8$Mn$_4$ at 1.5 and 300 K are presented in Figs. 7, 8, and 9, respectively. On the basis of the analysis of the neutron spectra at
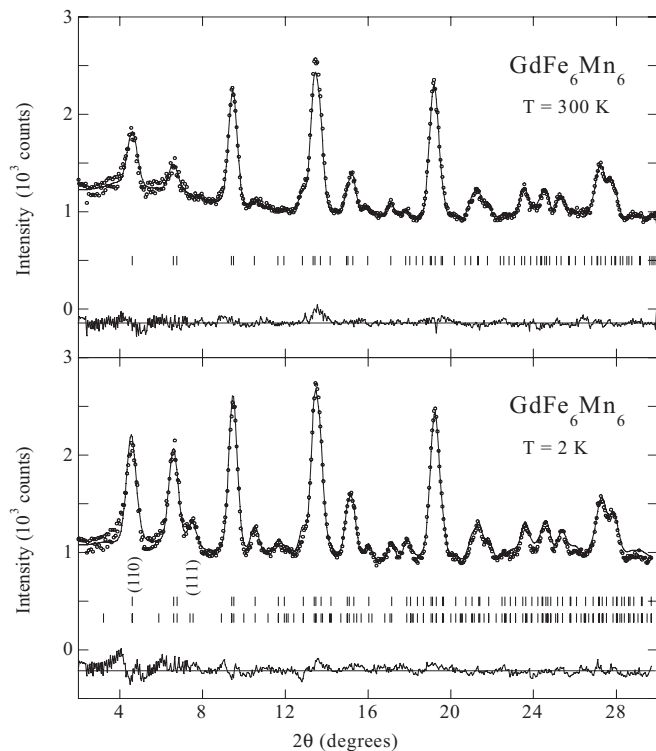
FIG. 7. Observed (points), Rietveld method fit (solid line), and difference (bottom) neutron-diffraction profiles for GdFe$_6$Mn$_6$ measured at 2 and 300 K at D4 (λ=0.50 Å). The first and second series of tick marks correspond to the positions of the allowed Bragg reflections: top, nuclear+ferromagnetic; bottom, AF 3d component.

FIG. 8. Observed (points), Rietveld method fit (solid line), and difference (bottom) neutron-diffraction profiles for TbFe$_4$Mn$_8$ measured at 1.5 and 300 K at D1B (λ=2.52 Å). The first and second series of tick marks correspond to the positions of the allowed Bragg reflections: top, nuclear; bottom, AF 3d component.

1.5 K, the main refinement parameters are presented in Table II. The reliability factors for DyFe$_4$Mn$_8$ and RFe$_2$Mn$_{10}$ alloys for R=Gd, Tb, and Dy are not completely satisfactory. These samples were found to contain nonoverlapping peaks of the β-Mn impurity phase that affect the analysis of these neutron-diffraction spectra.

For the binary compound TbMn$_{12}$, the best agreement between calculated and observed intensities below T_N=120 K corresponds to a noncollinear AF structure of the 3d moments in the basal plane, of the type previously found in YMn$_{12}$.[5] Furthermore, below 4.5 K, the Tb site develops an F component in the basal plane, reaching 7.73μ_B at 1.5 K. It is worth noting that the components of the R magnetic moment within the plane perpendicular to the unique axis of the tetragonal crystalline structure cannot be determined from powder diffraction due to symmetry considerations.[13] The propagation vector of the Mn sublattice is $\mathbf{Q}$=(1,0,0), while that of the Tb sublattice is $\mathbf{Q}$=(0,0,0). This is consistent with the existence of two independent ordering temperatures and with the planar anisotropy of Tb (the second-order Stevens coefficient $\alpha_J<0$ and the second-order crystal-field parameter $A_{20}<0$). The value of the Tb magnetic moment is lower than that of the free ion value (9μ_B), but higher than the one previously reported (6.5μ_B).[1] This reduction could be related to crystal-field effects, as observed in other RFe$_x$Mn$_{12-x}$ (R=Nd, Ho, and Er)[8] and in other tetragonal Tb intermetallic systems.[14]

However, with the addition of a small amount of Fe (x=2 and 4), the Tb F component disappears and the
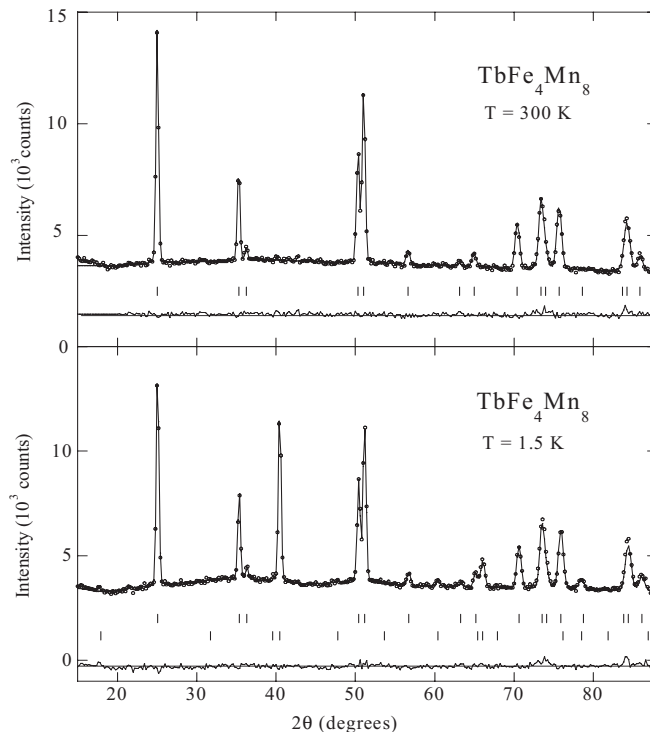
magnetic structure is similar to the structure of the corresponding Y compounds.[5] The same structure is found for DyFe$_x$Mn$_{12-x}$ (x=2 and 4). As can be observed in Fig. 8 for TbFe$_4$Mn$_8$, the neutron-diffraction pattern at 1.5 K shows diffuse scattering. The difference in patterns between the 1.5 K powder neutron-diffraction pattern and patterns collected close to the spin-glass temperature (T_f=50 K for TbFe$_4$Mn$_8$) and above allows us to conclude that the existence of this diffuse scattering seems to be associated with short-range interactions related to the 3d magnetic moments, also detected in magnetization measurements (see above).

In contrast, the F component at the 2a site remains for the Gd compounds (x=2, 4, and 6) and, additionally, another F component appears at the highest Fe concentration site (8f), antiparallel to the moment of the Gd sublattice. Due to the low resolution of the D4 diffractometer, we assumed the same AF structure found in the corresponding Y, Tb, and Dy compounds for the 8i and 8j sites, and an antiparallel alignment of the 8f and Gd magnetic moments, as is commonly observed in intermetallic compounds of rare earths and transition-metal alloys. One puzzling feature is the angle between the direction of the Gd magnetic moment and the c axis of the tetragonal structure (see Table II and Fig. 10). Approximately, the same angle (33.4°) has been found in GdMn$_{12}$ from NMR and magnetic measurements[2] and in GdFe$_4$Al$_8$ (44°).[15] It is worth noting that the F component at the 8f site does not appear in the corresponding Y compounds. The reason for this existence in GdFe$_x$Mn$_{12-x}$ (x=2,
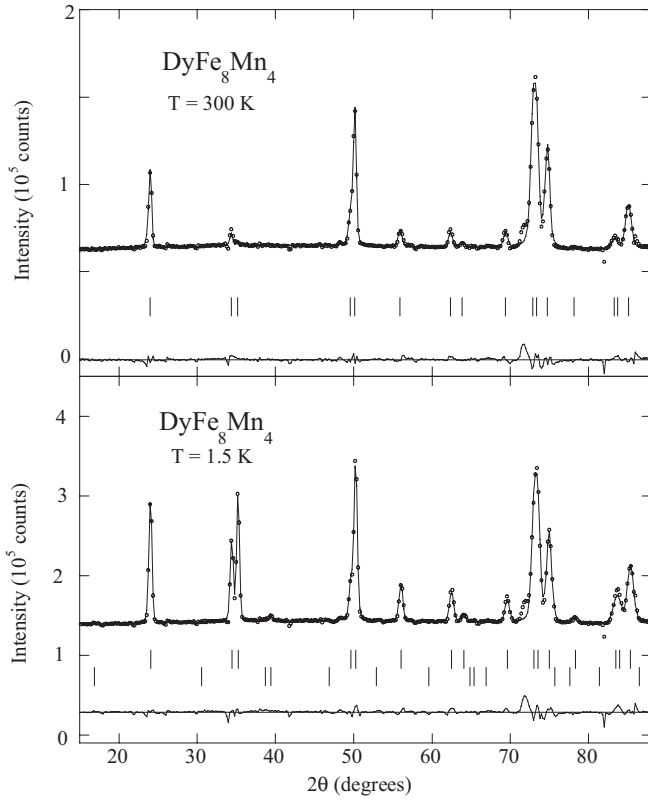
FIG. 9. Observed (points), Rietveld method fit (solid line), and difference (bottom) neutron-diffraction profiles for DyFe$_8$Mn$_4$ measured at 1.5 and 300 K at D1B ($\lambda=2.52$ Å). The first and second series of tick marks correspond to the positions of the allowed Bragg reflections: top, nuclear+ferromagnetic; bottom, AF 3d component.

4, and 6) compounds could be attributed to intra-atomic exchange interaction 4f-5d and 5d-3d band hybridization. We investigated the change in 5d-3d band hybridization by measuring XAS at the Gd-L_{III} edge 7243 eV (2$p_{3/2}$-5d transitions) at room temperature. The normalized XAS at the Gd-L_{III} edge for all investigated GdFe$_x$Mn$_{12-x}$ ($x=2$, 4, and 6) compounds are shown in Fig. 11. The well-known relationship between the energy dependence of the x-ray absorption, $\mu(E)$, and the angular-momentum-projected density of states, $\rho(E)$, is given by

$$\mu(E) = f_{at}(E)\rho(E),\qquad(1)$$

where $f_{at}(E)$ is a smoothly varying function of the probed atom that does not depend on its local environment.[16,17] There is a reduction in the absorption white line, increasing the Fe content from $x=2$ to $x=6$. According to Eq. (1), this reduction can be interpreted as being due to progressive delocalization of the Gd 5d band states and hence greater 5$d-3d$ band hybridization. This feature could favor the appearance of a ferromagnetic arrangement at the 8f sites due to an increase in the 8f-8f coupling through the first next neighbors: the 4f ions at the 2a sites.

The temperature dependence of the Gd magnetic moment and the intensities associated with the (110) and (111) reflec-

TABLE II. Magnetic parameters obtained from the neutron-diffraction profile refinements of RFe$_x$Mn$_{12-x}$ at 1.5 K: magnetic moment at the sites 2a, 8i, 8j, and 8f (μ_{2a}, μ_{8i}, μ_{8j}, and μ_{8f}); angle between the rare-earth magnetic moment and the c axis (θ_{2a}); and reliability factors R_B^N and R_B^M.

	μ_{2a} (μ_B)	θ_{2a} (deg)	μ_{8i} (μ_B)	μ_{8j} (μ_B)	μ_{8f} (μ_B)	R_B^N (%)	R_B^M (%)
GdFe$_2$Mn$_{10}$	6.7(1)	23(6)	1.10(8)	1.05(7)	0.14(4)	10.6	17.4
GdFe$_4$Mn$_8$	6.6(1)	33(2)	1.34(5)	1.24(4)	0.53(3)	6.9	8.7
GdFe$_6$Mn$_6$	7.0(1)	30(3)	1.34(9)	1.40(6)	0.83(8)	8.9	12.4
TbMn$_{12}$	7.73(7)	90	0.8(2)	0.8(1)	0.1(2)	4.7	7.6
TbFe$_2$Mn$_{10}$			0.66(7)	1.22(6)	0.24(6)	5.4	15.2
TbFe$_4$Mn$_8$			1.17(6)	1.40(5)	0.49(7)	9.6	7.8
TbFe$_6$Mn$_6$	7.80(8)	90	1.33(9)	0.85(8)	1.24(8)	9.2	13.3
TbFe$_8$Mn$_4$	8.3(1)	90	0.87(9)	1.0(2)	1.0(1)	5.6	6.3
DyFe$_2$Mn$_{10}$			1.0(5)	1.0(4)	0.3(4)	10.4	18.8
DyFe$_4$Mn$_8$			1.4(2)	1.3(1)	0.3(2)	7.4	17.2
DyFe$_6$Mn$_6$	6.8(1)	20(3)	1.0(3)	1.2(2)	0.64(7)	6.0	11.9
DyFe$_8$Mn$_4$	9.5(1)	67(2)	1.0(2)	1.1(1)	1.12(7)	5.2	8.7

tions in the low angle region of the diffractogram (see Fig. 7) are presented in Fig. 12 for GdFe$_6$Mn$_6$. The peak (111) suddenly appears below $T_N\sim200$ K, indicating a cooperative AF ordering of the 3d sublattice corresponding to the sites 8i and 8j and an F ordering at the site 8f. Due to the low value of the magnetic moment at the 8f site, we are close to the experimental resolution limit, but it seems that the T_C of the 8f site is similar to the T_N of the 8i and 8j sites. To monitor the onset of ordering at this site, a more selective technique such as x-ray resonant magnetic scattering would be needed. In contrast, below ~150 K the intensity of the (110) peak grows continuously, being indicative of the appearance of progressive polarization of the paramagnetic Gd moments by the exchange field created by the 8f F ordered moments. Figure 12 also shows the temperature evolution of the Gd magnetic moment together with the theoretical value calculated for the case of a paramagnetic system under the action of a molecular field ($B_{3d-4f}=48$ T, which was calculated from
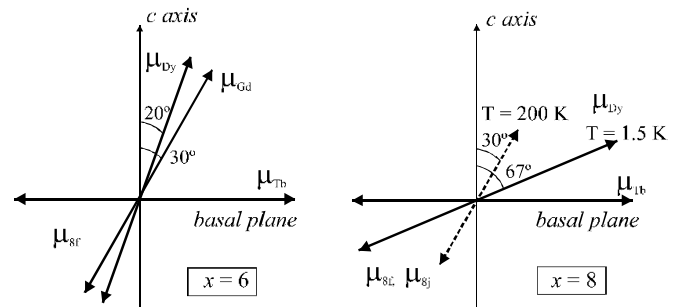

FIG. 10. Schematic representation of the magnetic-moment orientation for the rare earths ($\mu_{Gd}, \mu_{Tb}, \mu_{Dy}$) and for the transition metals at the sites F coupled: μ_{8f} in RFe$_6$Mn$_6$ (R=Gd, Tb, and Dy) and μ_{8f} and μ_{8j} in RFe$_8$Mn$_4$ (R=Tb and Dy) at two temperatures.
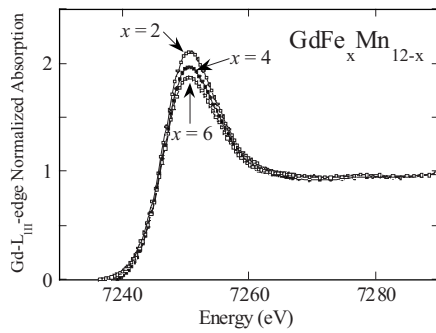
FIG. 11. Comparison of the normalized Gd-L_{III} edge XAS spectra through the GdFe$_x$Mn$_{12-x}$ series for $x=2$, 4, and 6.

heat-capacity measurements).[6] The good agreement indicates that there is no cooperative order in the Gd sublattice due to Gd-Gd interaction, although polarization is evidenced below 150 K. The temperature dependence of the magnetic moment found in GdFe$_6$Mn$_6$ increases progressively when the temperature is lowered and is quite different from that found in other Gd-based intermetallic systems,[18] in which magnetic moment increases abruptly just below the ordering temperature to then reach saturation at low temperatures. This is due to mutual coupling between the Gd ions, instead of 3*d*-4*f* polarization, as is suggested in GdFe$_x$Mn$_{12-x}$ from the present study. Owing to the antiparallel alignment between the Fe/Mn magnetic moments ($\sim 0.83 \mu_B$) at the sites 8*f* and of the Gd ions ($7.0 \mu_B$) (see Fig. 10), there is a compensation point at around 100 K (8*f*: $0.83 \times 4 = 3.3 \mu_B$ which is the magnitude of the magnetic moment of the Gd ion at around 100 K, see Fig. 12), leading to the minimum observed in the M/H measurements (see Fig. 3) which corresponds to this crossover point.

The same phenomenon is encountered in TbFe$_6$Mn$_6$ and DyFe$_6$Mn$_6$. The magnetic structure is AF in the basal plane for the 8*i* and 8*j* sites, the same as in YFe$_6$Mn$_6$, and F at the 8*f* and 2*a* sites, both F components being antiparallelly oriented. For all the temperatures, the magnetic moments lie in the basal plane for the Tb compound, although the Dy magnetic moment in DyFe$_6$Mn$_6$ forms an angle of 20° with the *c*
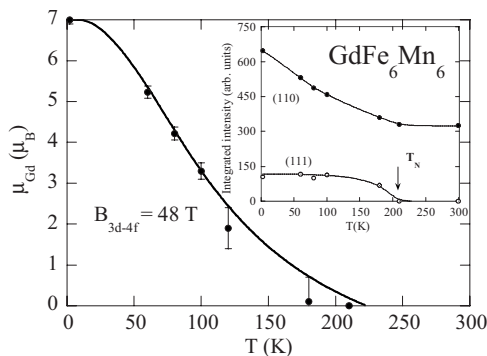

FIG. 12. Magnetic moment of Gd derived from neutron-scattering experiments for GdFe$_6$Mn$_6$ together with the theoretical calculation as described in the text. The inset shows the temperature dependence of the integrated intensity for (110) and (111) reflections. T_N is the Néel temperature.
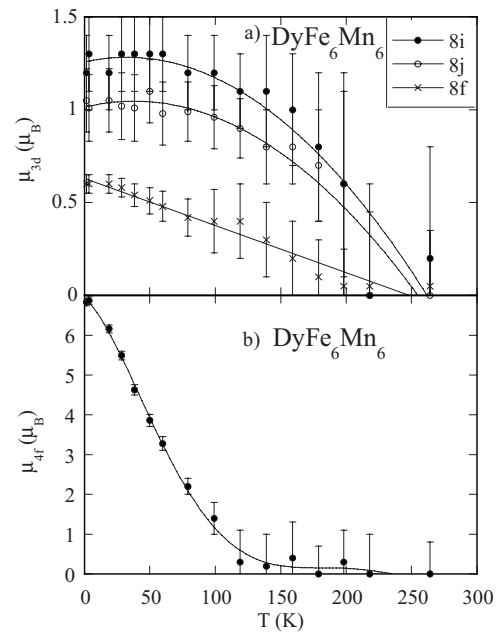

FIG. 13. (a) Magnetic moment of the Fe/Mn atoms at the sites 8*i* (●), 8*j* (○), and 8*f* (×) and (b) magnetic moment of Dy (●) derived from neutron-scattering experiments for DyFe$_6$Mn$_6$.

axis (see Table II and Fig. 10). This different orientation between the magnetic moments in Tb and Dy compounds is explained by the different value of α_J: being both negative (basal plane anisotropy), that of Dy is smaller and we have to consider the fourth-order terms in the CEF potential, as in RFe$_{11}$Ti.[19] From the temperature dependence of the magnetic moments, presented in Fig. 13 for DyFe$_6$Mn$_6$, we conclude that at T_N (8*i* and 8*j*) or T_C (8*f*) (~ 230 K for TbFe$_6$Mn$_6$ and ~ 250 K for DyFe$_6$Mn$_6$) the 3*d* sublattice orders cooperatively at the 8*i* and 8*j* sites in the same AF structure as in YFe$_6$Mn$_6$,[5] while the rare-earth ion remains paramagnetic. Below approximately 100 K (for DyFe$_6$Mn$_6$) or 120 K (for TbFe$_6$Mn$_6$), where the molecular field overcomes thermal disorder, the rare-earth sublattice develops a long-range F ordering due to the polarization by the molecular field of the F ordered magnetic moment in the 8*f* sublattice, as we have seen in magnetization measurements. On the other hand, it is worth noting that this polarization is also present in GdFe$_x$Mn$_{12-x}$ for Fe concentrations $x=2$ and $x=4$, in addition to $x=6$, meaning that the CEF interaction present in Tb and Dy compounds prevents the appearance of the long-range rare-earth F ordering for $x=2$ and $x=4$.

For the highest Fe concentration studied, in TbFe$_8$Mn$_4$ (see Fig. 14) and DyFe$_8$Mn$_4$, both with $T_C \sim 300$ K, an F component develops at the sites 8*j* and 8*f* (with predominance of Fe), both parallel and oriented antiparallel to the 2*a* site F component originating from the rare earth. The AF arrangement in the basal plane only remains at the 8*i* site (mostly occupied by Mn) below ~ 150 K [see Fig. 14(a)], once again showing the coexistence of ferro- and antiferromagnetism at different 3*d* crystallographic sites. In this case, the 3*d*-4*f* exchange field is large enough, the 3*d* sublattice being globally F, to develop the rare-earth F component below T_C [see Fig. 14(b)]. Once more for TbFe$_8$Mn$_4$, all the
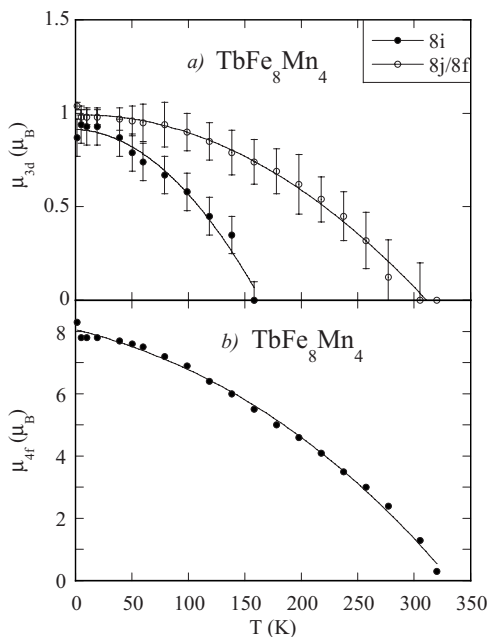
FIG. 14. (a) Magnetic moment of the Fe/Mn atoms at the sites 8*i* (●) and 8*j*/8*f* (○) and (b) magnetic moment of Tb (●) derived from neutron-scattering experiment for TbFe$_8$Mn$_4$.

moments are in the basal plane at every temperature below T_C. In DyFe$_8$Mn$_4$, however, the Dy magnetic moments form an angle of 67° with the *c* axis of the tetragonal structure at 1.5 K and show a spin reorientation transition (SRT) (see Fig. 10): this angle decreases with increasing temperature (being 30° at 200 K). The Fe substitution modifies the electronic density around the 2*a* site (changing the CEF parameters) and leads to an increase of the second-order CEF parameter that favors planar anisotropy (with *x*=6 the angle was 20° at 1.5 K). The origin of the SRT could reside in the fact that Fe anisotropy (axial) dominates the Dy anisotropy (planar) as the temperature increases.

From the combined analysis of all the experimental data obtained in the present work, we established the magnetic phase diagram of RFe$_x$Mn$_{12-x}$ (R=Gd, Tb, and Dy) compounds (see Figs. 15 and 16 for R=Gd and Tb, respectively; the magnetic phase diagram for R=Dy is similar to that corresponding to Tb). The binary compound TbMn$_{12}$ is an itinerant AF in the temperature range $T_R < T < T_N$ (AF-I, noncollinear magnetic moments in the basal plane favored by the Mn anisotropy, as in YMn$_{12}$). At T_R=4.5 K, there is a second-order phase transition with an ordering of the Tb sublattice in the basal plane due Tb-Tb exchange interaction. With a small amount of Fe, the rare earth no longer orders cooperatively through R-R interactions. The extra exchange field that appears due to the F ordering of Fe at the 8*f* site suppresses the magnetic ordering of the R sublattice. The R moments thus behave as a paramagnetic system in an internal field that polarizes the R magnetic moments. We may say that the R moments are so polarized that there is no more entropy left to allow for an order-disorder cooperative phase transition. This is manifested in Gd (*x*=2, 4, and 6) and Tb and Dy (*x*=6) compounds at low temperatures, where thermal disorder is overcome. There exists mutual polariza-
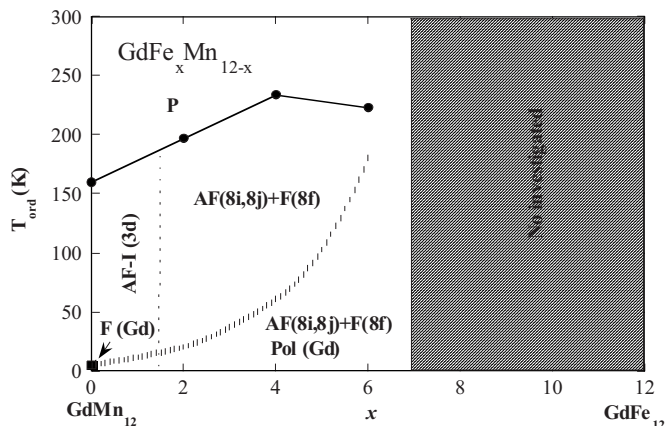

FIG. 15. Magnetic phase diagram of GdFe$_x$Mn$_{12-x}$. T_N (●) has been taken from Ref. 6 and T_R (■) has been taken from Ref. 2. The curve with vertical lines represents the temperature at which the mutual polarization between the Gd and the 8*f* magnetic moment is clearly evidenced. For *x*<2, not investigated in this work, we assume the same structure as found in YMn$_{12}$ and in TbMn$_{12}$.

tion between the two sublattices; the R polarization enhances the F component at the 8*f* site, preferentially occupied by Fe. The long-range ordering of the R sublattice is frustrated in Tb and Dy (*x*=2 and 4) compounds because of the competition between the CEF and the R-3*d* exchange interaction, the latter not being sufficiently strong. Spin-glass behavior is observed at low temperatures. This disorder effect has also been observed in RFe$_x$Mn$_{12-x}$ with R=Nd,Ho,Er.[8] Thus, Tb and Dy compounds (*x*=2 and 4) are noncollinear antiferromagnets (AF-II, as in YFe$_x$Mn$_{12-x}$).

A different situation arises in the rich Fe composition compounds (*x*=8), in which the strong exchange field acting on the rare earth is responsible for its ordering at T_C, antiferromagnetism only appearing at the 8*i* site, populated with a higher Mn content, and below 150 K. This is different from the case of the Y compounds, in which the AF component
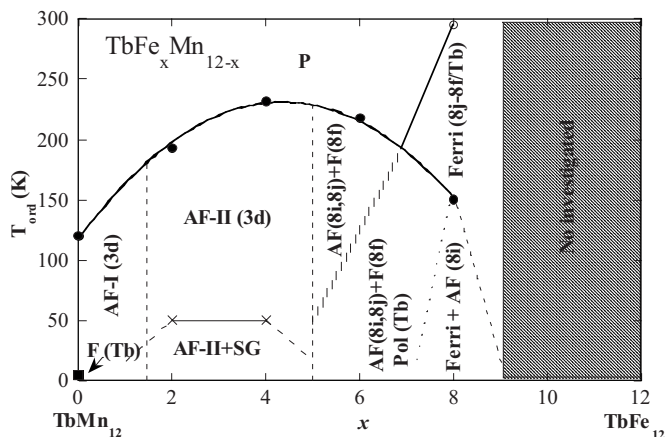

FIG. 16. Magnetic phase diagram of TbFe$_x$Mn$_{12-x}$. T_N (●), T_R (■), and T_C (○) (taken from Ref. 6) and T_f (×). The curve with vertical lines represents the temperature at which the mutual polarization between the Tb and the 8*f* magnetic moment is clearly evidenced.

exists at all three $3d$ sites. This is another proof of the mutual enhancement between the $3d$ and $4f$ sublattices.

IV. CONCLUSIONS

The physical behavior of $R\text{Fe}_x\text{Mn}_{12-x}$ depends very much on the relative strength of intra- and intersite exchange interactions. The $R\text{Fe}_x\text{Mn}_{12-x}$ family of compounds is particularly interesting because the crystallographic structure contains several sites which are selectively occupied by the transition-metal Fe/Mn atoms. While the binary $R\text{Mn}_{12}$ compounds present two phase transitions with two independent ordering temperatures for the $3d$ and R sublattices, the magnetic behavior of $R\text{Fe}_x\text{Mn}_{12-x}$ ($R=\text{Gd},\text{Tb},\text{Dy}$) provides strong evidence for the coexistence of ferro- (Fe atoms preferentially at site $8f$) and antiferromagnetic orderings (Mn atoms preferentially at sites $8i$ and $8j$); these ordering temperatures coincide when the Fe content reaches values of around $x=6$. Dilution with Fe of the antiferromagnetically ordered $R\text{Mn}_{12}$ system enhances the exchange field acting on the rare-earth ions and competition between the $4f$-$4f$ and $3d$-$4f$ exchange interactions occurs, leading to the disappearance of the cooperative ordering of the R sublattice and the appearance of mutual polarization between the R and $3d$ sublattices. Further studies are needed in the range of low Fe composition in order to study the array of phenomena involved in this competition.

*Also at Departamento de Física, Universidad de Oviedo, Campus de Viesques, Edificio Este, 33203 Gijón, Spain. Email address: pique@uniovi.es

[1] J. Deportes, D. Givord, R. Lemaire, and H. Nagai, Physica B & C **86-88**, 69 (1977).

[2] N. Okamoto, H. Nagai, H. Yoshie, A. Tsujimura, and T. Hihara, J. Magn. Magn. Mater. **70**, 299 (1987).

[3] J. A. Paixão, M. Ramos Silva, S. A. Sørensen, B. Lebech, G. H. Lander, P. J. Brown, S. Langridge, E. Talik, and A. P. Gonçalves, Phys. Rev. B **61**, 6176 (2000).

[4] S. Langridge, J. A. Paixão, N. Bernhoeft, C. Vettier, G. H. Lander, Doon Gibbs, S. A. Sørensen, A. Stunault, D. Wermeille, and E. Talik, Phys. Rev. Lett. **82**, 2187 (1999).

[5] C. Piqué, E. Abad, J. A. Blanco, R. Burriel, and M. T. Fernández-Díaz, Phys. Rev. B **71**, 174422 (2005).

[6] C. Piqué, J. A. Blanco, R. Burriel, E. Abad, and M. Artigas (unpublished).

[7] W. Mao, J. Yang, B. Cheng, and Y. Yang, Solid State Commun. **109**, 655 (1999).

[8] M. Morales, M. Bacmann, P. Wolfers, D. Fruchart, and B. Ouladdiaf, Phys. Rev. B **64**, 144426 (2001).

[9] J. B. Yang, W. B. Yelon, W. J. James, Q. S. Cai, D. Eckert, A. Handstein, K. H. Müller, and Y. C. Yang, Phys. Rev. B **65**, 064444 (2002).

[10] J. Stankiewicz, J. Bartolomé, and D. Fruchart, Phys. Rev. B **67**, 092409 (2003).

[11] M. G. Shelyapina, M. Morales, M. Bacmann, F. Baudelet, D. Fruchart, C. Giorgetti, E. K. Hlil, G. Krill, and P. Wolfers, J. Alloys Compd. **368**, 84 (2004).

[12] J. Rodriguez-Carvajal, Physica B **192**, 55 (1993).

[13] G. Shirane, Acta Crystallogr. **12**, 282 (1959).

[14] J. A. Blanco, D. Gignoux, and D. Schmitt, Z. Phys. B: Condens. Matter **89**, 343 (1992).

[15] I. Felner and I. Nowik, J. Phys. Chem. Solids **39**, 951 (1978).

[16] J. E. Müller and J. W. Wilkins, Phys. Rev. B **29**, 4331 (1994).

[17] A. Bianconi, in *X-ray Absorption: Principles, Applications, Techniques of EXAFS, SEXAFS and XANES*, edited by D. C. Koningsberger and R. Prins (Wiley, New York, 1988).

[18] J. A. Blanco, J. I. Espeso, J. J. Garcia-Soldevilla, J. C. Gomez Sal, M. R. Ibarra, C. Marquina, and H. E. Fischer, Phys. Rev. B **59**, 512 (1999).

[19] C. Abadía, P. A. Algarabel, B. García-Landa, M. R. Ibarra, A. Del Moral, N. V. Kudrevatykh, and P. E. Markin, J. Phys.: Condens. Matter **10**, 349 (1998).